Sustainable Structures and Materials, *Vol. 4, No .2, (2022) 01-18*

DOI: https://doi.org/10.26392/SSM.2022.04.02.001

Experimental Study of Pile-Sandy Soil Interaction of Integral Abutment Bridges with Low-Cyclic Lateral Load

Yizhou Zhuang,[1] Zelun Chen,[1] Said M. Easa,[2]* Yingang Guo,[1] Fuyun Huang,[3] and Zengfeng Li[3]

[1]College of Civil Engineering, Zhejiang University of Technology, Hangzhou 310014, Zhejiang, China
[2] Department of Civil Engineering, Ryerson University, M5B 2K3, Toronto, Ontario, Canada
[3] College of Civil Engineering, Fuzhou University, Fuzhou 350108, Fujian, China
**Correspondence: seasa@ryerson.ca*

(Received November 1, 2021, Revised January 1, 2022, Accepted January 5, 2022)

ABSTRACT. *This paper experimentally investigates the mechanism and deformation of circular and rectangular reinforced concrete (RC) piles of integral abutment bridges (IAB) in a sandy environment. Pseudo-static tests of the RC piles under low-cyclic loading were conducted to simulate the periodic displacement of the IAB due to temperature changes. A lateral displacement load was applied on the pile head and the characteristics of energy dissipation, strain, bending moment, lateral displacement, and pile damage were analyzed. The results show that the ratio of reinforcement and the shape of the section significantly influence the energy dissipation and RC pile ductility. The ratio of reinforcement (1.6% to 3.2%) is suitable for the RC pile, providing excellent energy dissipation and ductility. Under the action of the reciprocating load, the concrete pile has apparent pile body failure in the range of 3 to 7 times of pile diameter and buried depth. The earth pressure around the pile is mainly distributed in 0 to 10 times the pile diameter and the buried depth. Among them, the earth pressure in the shallow soil is the most considerable, and the maximum value appears around four times the pile diameter. The lateral resistance of the RC pile accounts for over 50% of the whole soil-pile system in the elastic stage. However, the resistance distribution of the surrounding soil of the pile is more than 50% in the latter stages. Furthermore, the performance of the circular RC pile was better than the rectangular one. It is recommended to use the circular pile in bridge design when the RC pile is used as the foundation of IABs, especially in areas with high seismic fortification levels.*

Keywords: Energy; Integral abutment bridge; Pile-soil interaction; RC pile.

1. INTRODUCTION

Integral Abutment Bridges (IABs) have been widely used for their robustness, seismic resistance, and economical life-cycle maintenance costs in North America and Europe. However, the IAB design is complicated, especially for the lateral deformation of the pile. HP steel piles have high strength and excellent deformation capacity, which is suitable for seismic resistance and reduces thermal stress in the abutment and superstructure [1]. Therefore, HP steel piles are widely studied and applied to the bridge foundation of IABs in many countries, see Girion et al. [2], Far et al. [3], Salman et al. [4], Gama and Almeida [5], and Abendroth et al. [6]. Reinforced concrete (RC) piles are cheaper than HP steel piles for bridge foundation in China, but the research on the mechanical behavior of the RC pile is not deep enough, as indicated by Magbool [7]. In recent years, IABs have been more popularized in China, where the RC pile are used for the IAB foundation, see Hong and Peng [8] and Zhuang et al. [9]. The strength and deformation capacity of the RC pile foundation is weaker than that of the HP steel pile, and the difference in the performance of the

RC pile and the HP steel pile is lack of in-depth study. The design and calculation methods for IABs are not given in the Chinese General Specification for Design of Highway Bridges and Culverts [10]. The *Technical Code for Building Pile Foundations* by the Ministry of Construction of the People's Republic of China [11] is mainly based on elasticity, small deformation. It is not easy to suitable the engineering requirements like the IABs and the existence of sizeable nonlinear deformation. Therefore, it is necessary to experiment on the lateral bearing characteristics of IABs RC pile based on large displacements, according to Huang et al. [12].

At present, there are research results on the dynamic response and bearing characteristics of various kinds of piles in soft soil under earthquake, see Makris and Gazetas [13], Mylonakis and Nikolaou [14], Anoyatis et al. [15], Chidichimo et al. [16], Shamsabadi et al. [17], and Govindaraju et al. [18]. The relationship between the energy dissipation capacity of the pre-stressed high-strength concrete (PHC) piles and the amount of steel bars through the low-cyclic load test of PHC piles were studies by Chung [19], Park et al. [20], and Park [21], respectively. The studies explored the relationship between temperature and mechanical properties of the PHC pile through the prototype site test and FEM. Zhuang [9] and Huang [22] carried out an experimental study on the influence of prestressing degree and thickness of the PHC piles on the lateral compression deformation performance of PHC piles.

Qian [23] and Zhuang et al. [24] carried out pseudo-static tests on four PHC pipe piles under low-cycle reciprocating load. They obtained a practical calculation method for the lateral deformation considering the interaction between pile and soil around PHC pipe based on displacement. Wang et al. [25] conducted a shaking table test for the interaction among the micro-soil-dynamic forces of reaming at the back of a new type of semi-integral abutment seamless bridge abutment. They obtained the P-Y hysteretic curves of micro-soil-dynamic forces of reaming under different reaming parameters. Xu et al. [26] conducted shaking table tests on micro pile's dynamic response characteristics, analyzed the P-Y curve's applicability in the dynamic interaction between micro pile and soil, and derived the dynamic P-Y curve suitable for micropile-sandy soil condition. Murugan et al. [27] experimentally studied the load deformation, stiffness decline, and energy dissipation of a pile under cyclic lateral load. Zhao [28] introduced a small model RC pile that reproduced the failure mechanism of the RC pile under lateral load by forming actual tensile cracks and plastic hinges using nonlinear finite element model. Cheng et al. [29]. The experimental results of dynamic response characteristics of RC micro piles in SJABs show that the maximum strain response of piles was observed at the buried depth of 4.2 D (D is the diameter of the pile). The RC piles are widely used for IABs in China. Therefore, it is essential to study the lateral deformation of RC piles and the interaction characteristics of piles and soils.

The calculation methods for the lateral reaction coefficient of the foundation, which are based on the elastic linear small deformation include the Zhang's method, the *C* method, and the most used *M* method [11]. For large nonlinear deformations exceeding 10 mm, these calculation methods are challenging to suffice the requirements of the IABs for lateral deformation of the pile. This paper evaluates the stress deformation performance, failure mode and pile-soil interaction, and evaluation of seismic resistance capacity of the RC pile using an indoors low-cyclic lateral loading test of the model piles in sand.

2. EXPERIMENTAL DESIGN

2.1 RC Pile Models

In this experiment, 4 RC model piles were designed and fabricated, and a Pseudo-static test was carried out. There are two types of sections of the model pile: circular and rectangular, as shown in Fig. 1(a) and 1(b). M-1, M-2, and M-3 are circular piles with a pile length of 3,500 mm and a pile diameter of 155 mm. M-4 is a rectangular pile with a pile length of 3,500 mm and a section size of 155 x 217 mm. The scale ratio of the model to the prototype, based on the scale of the pile diameter, is 0.31 ($S = L_m / L_p = 155 / 500 = 0.31$). In this paper, based on the material size, D is defined as 155 mm. The similarity ratio S_E of the initial mass density similarity ratio S_{P0} and the elastic modulus is 1. The thickness of the protective layer of the

model pile is 20 mm, the reinforcement ratio is over 0.65%, and the ordinary circular double-legged hoop is used in the form of stirrups. As shown in Fig. 1(c), the hot plain bar with a diameter of 6 mm is used, and the stirrup spacing between the top and bottom of the pile is 100 mm. The spacing of the stirrups in the middle non-encrypted area is 120 mm, which suffices the code requirements by the Ministry of Transport [30]. The reinforcement of the model piles is shown in Table 1.

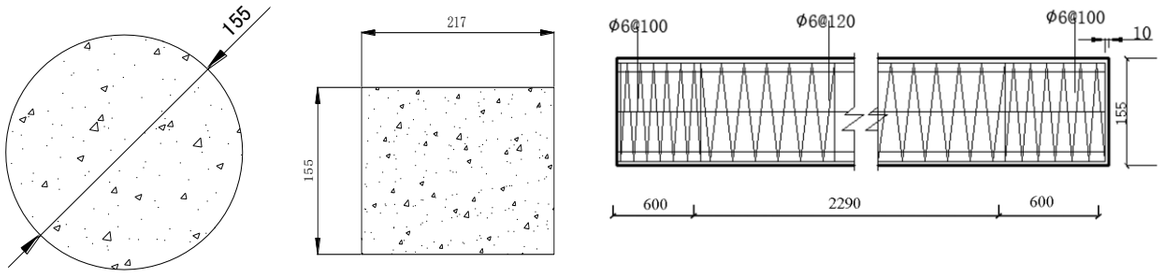

(a) Sections M-1 to M-3 (b) Section M-4 (c) Pile model

Fig – 1: Pile section form and diagram of pile model (unit: mm)

Table - 1: Characteristics of model piles

Numbe	ρ	Reinforcement	Length	Number of stirrups
M-1	0.8%	6Φ6	3400	30
M-2	1.6%	6Φ8	3400	30
M-3	3.2%	4Φ14	3400	30
M-4	1.6%	6Φ10，2Φ8	3400	30

Due to the small diameter and long length of the model pile, it is difficult to cast concrete and dismantle the mold. Therefore, the circular pile uses PVC as a formwork like shown in Fig. 2(a), while the rectangular pile uses the formwork with wood. The steel cage shown in Fig. 2 (b) is placed in the PVC pipe. Then, the PVC pile and the steel cage were placed vertically, fixed with wooden strips, and finally the concrete was poured. For the rectangular pile, the plank can be used, and the steel cage is placed. Finally, the concrete was cast.

(a) Pipe formwork (b) Steel cage

Fig – 2: Steel cage and PVC pipe formwork

Following the mix design [31, 32], the mix proportions of the C40 self-compacting concrete (kg.m^3) were as follows: cement (221), mineral (147), fly ash (123), sand (827), stone (828), reducing-agent water (13.4), and water (161). The mix proportion of self-compacting concrete in this experiment was 1:0.67:0.56:3.74:3.75:0.06:0.73. Note that self-compacting concrete with good flowability, construction performance, and filling properties was used in this experiment because the pile size was small, and the pouring was difficult. According to the mix proportions, several concrete test blocks were prepared, and the relevant parameters were obtained as: E (3.25x10^4 MPa), slump flow (680-695 mm), f_{cu} (47.6 MPa), and v (0.195). These properties satisfied the casting requirements.

2.2 Soil Container and Soil Parameters

Lou et al. [33] combined the finite element analysis with the test and found that when the ratio of the size of the local foundation plane to the size of the structural plane is greater than 5, the test error was significantly reduced. The diameter of the model pile in this batch test was 155 mm, and the size of the model soil box was determined according to the numerical simulation results. In this study, the rectangular soil container was selected, and its breadth, width, and height were 3 m, 2 m, and 4 m, respectively. The container was composed of steel plates of two specifications, including A (0.5 m × 3 m) and B (0.5 m × 2 m). The direction of bearing force was spliced by 8 pieces of A steel plate, and 8 pieces of B steel plate splice the one perpendicular to the direction above. The container is shown in Fig. 3(a).

As shown in Fig. 3(b), there are four angle sheets of steel welded at the bottom of the container to fix the model pile. Fill the container with sand until 0.4 m below the top of the pile. The physical parameters of the coarse sand are ω (natural moisture content) = 0.8%, e (void ratio) = 0.8, and φ (internal friction angle of the soil) = 35.86º, compressive strength = 28.9 MPa, average SPT blow count = 11, and relative compactness = 53%，measured using the geochemical test, as shown in Fig. 3(c).

(a) Container (b) Fixed Angle (c) Geotechnical test

Fig – 3: Test the fixed form of soil container and bottom of pile

2.3 Layout of Measuring Points

In this test, 20 strain gauges are arranged on each model pile and 10 strain gauges are placed on both sides of the pile. The first strain gauge is located at the boundary of the soil surface and the rest are distributed at an interval of 350 mm. Finally, the distance between the second strain gauge and the last strain gauge is 300 mm. The distribution is shown in Fig. 4(a). At the same time, 16 soil pressure gauges were arranged in the direction along the pile. The spacing was 350 mm and 8 soil gauges on each side. The distribution is shown in Fig. 4(b). Thirteen displacement gauges were set up in this test，and the detailed arrangement is shown in Fig. 4(c).

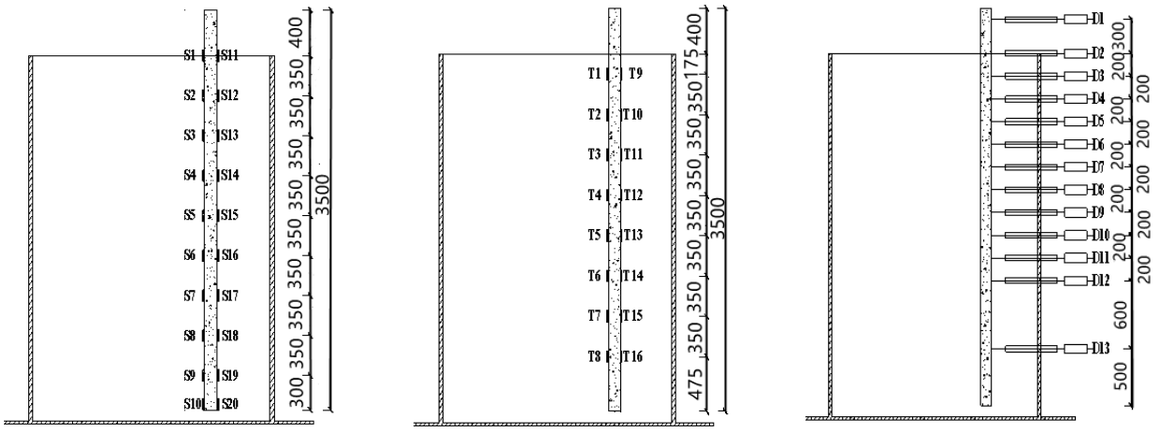

(a) Strain gauge (b) Soil pressure gauge (c) Displacement gauge

Fig -4: Layout of the sensor (unit: mm)

Since the displacement of each point of the pile is difficult to obtain by traditional measurement

methods, the following measurement method is used for this experiment. The nylon thread is tied to the octagonal nut, and the nut is bonded to the pile. Sand is filled into the container, and the sand filling is suspended and compacted when the filling height reaches a certain measuring point (in this experiment, the layer thickness for each compaction was 25 cm). As shown in Figure 5, the nylon wire is in direct contact with the soil during the test, which causes a significant error in the displacement measurement. Therefore, the nylon wire is passed through the steel pipe at the same horizontal line as the displacement measuring points. Also, the external displacement gauge is connected to keep the nylon thread in a tight state. The other end of the displacement gauge is fixed on an iron frame with a rubber band.

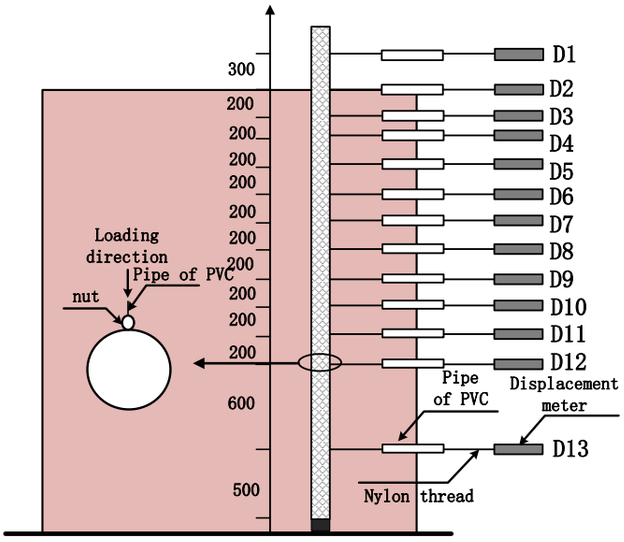

Fig -5: Arrangement of sensors (unit: mm)

2.4 Loading Device and Scheme

The lateral displacement of the pile head was controlled by MTS electro-hydraulic servo loading system, as shown in Fig. 6(a). The specific loading scheme is as follows:

1. At the initial stage of loading, the displacement of the pile head is applied according to 2 mm, 5 mm, 8 mm, and 10 mm, respectively.
2. When the displacement load range is 10 mm to 30 mm, the displacement increase increases by 5 mm (e.g., 10 mm, 15 mm, 20 mm, 25 mm, and 30 mm).
3. When the displacement load reached 30 mm, the displacement load increased by 10 mm.
4. The test was terminated when the lateral load is reduced to less than 85% of the ultimate load (the peak load at the elastic-plastic stage is shown in Fig.7), or the lateral displacement generated by the model exceeds the allowable value [34].

The loading rate is 1.0 mm/s when MTS applies the displacement load, and the load is cycled three times per stage to prevent the rebound of the steel bar. The collection time is guaranteed, and the load is held for 1 min before the loading direction is changed. The loading history is shown in Fig. 6(b) and 6(c).

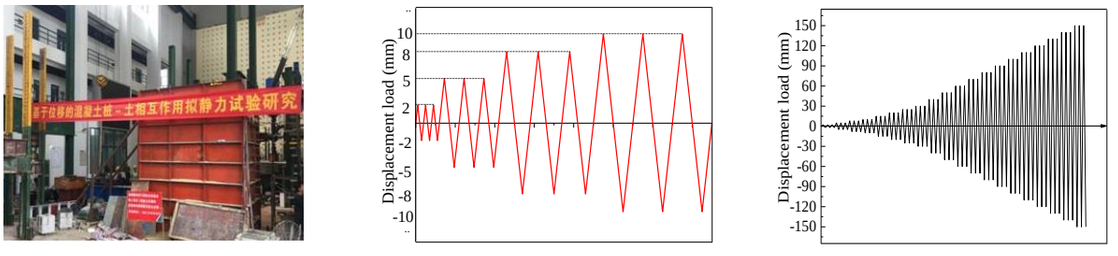

(a) Experimental setup (b) First stage loading history (c) Entire loading history

Fig – 6: Loading device and test history

3. ANALYSIS OF TEST RESULTS

3.1 Hysteresis Curve and Skeleton Curve

The hysteresis curve of the model pile is shown in Fig. 6. The shape of the hysteresis curve is the spindle, indicating that the pile (pile-soil system) has excellent energy dissipation capacity. The top load of M-1, M-2, and M-3 in Figures 7(a) to 7(c) reached 8 kN, 11k N, and 17 kN, respectively, indicating that the load-bearing performance of the pile foundation was improved with the reinforcement ratio. The corresponding displacement loads are 110 mm, 140 mm, and 130 mm, respectively. When the reinforcement ratio increases from 0.8% to 1.6%, the displacement load increases from 110 mm to 140 mm. In contrast, the displacement load does not increase when the reinforcement ratio increases from 1.6% to 3.2%. In addition, to make the ductility of the pile foundation the best, the corresponding reinforcement ratio should also be within a reasonable range, neither too low nor too high. Like the concrete flexural members, the pile foundation should be in a state of suitable reinforcement, and there should be no less reinforcement or excessive reinforcement. Comparing Figures 7(b) and 7(d), the top load of M-4 is about 19 kN at most, indicating that the rectangular pile can improve its load-bearing capacity compared with the circular pile. However, the maximum displacement load of M-4 can only reach 120 mm, indicating that the ductility of M-4 is lower than that of the circular pile.

Fig. 8 shows a comparison of the model piles skeleton curves, and Table 2 shows the model pile ductility coefficients. More details on these parameters can be found in [35]. As noted from Fig. 8(a), the ductility and bearing capacity of the model pile are related to the reinforcement ratio. As the reinforcement ratio increases, the bearing capacity is improved. When the bearing capacity reaches a specific value, while the displacement increases, the bearing capacity remains relatively stable for M-1 and M-2. However, the bearing capacity of M-3 is reduced significantly. The ductility coefficients of M-1 (4.18) and M-2 (5.49) are significantly better than that of M-3 (2.75), indicating that ductility does not increase as the reinforcement ratio increases.

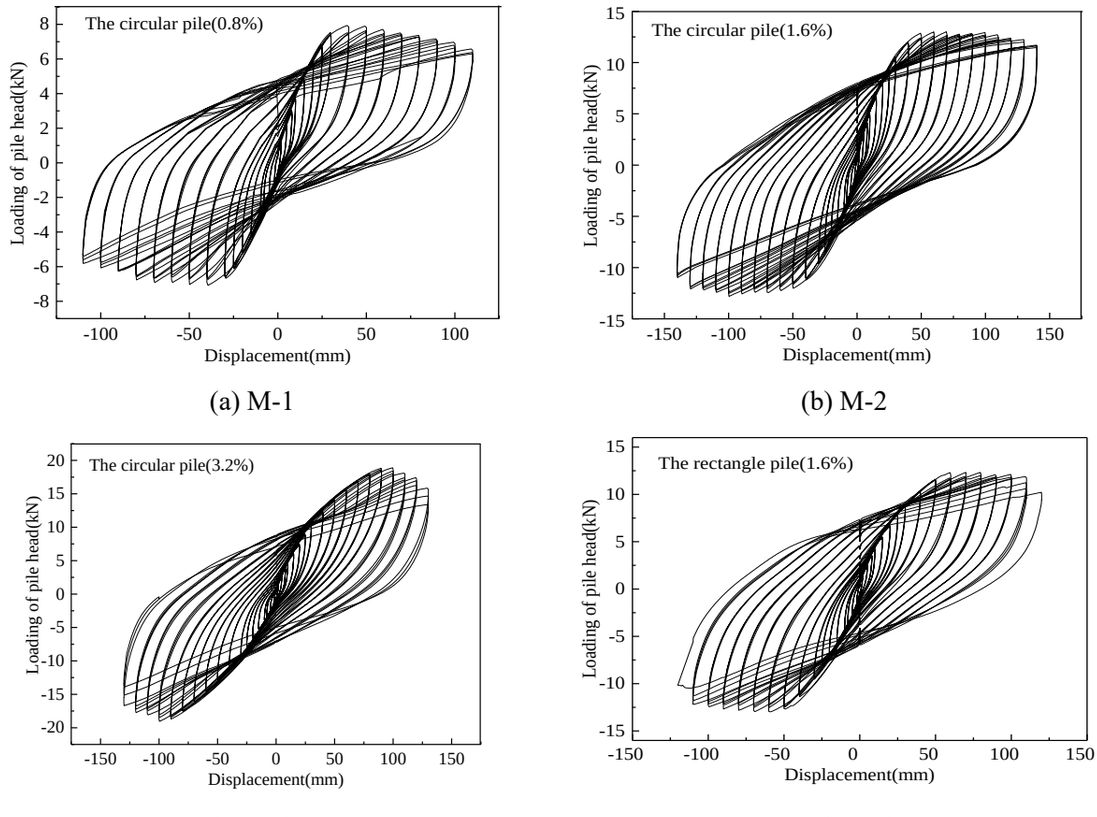

(a) M-1 (b) M-2

(c) M-3 (d) M-4

Fig – 7: Hysteretic loop of the models

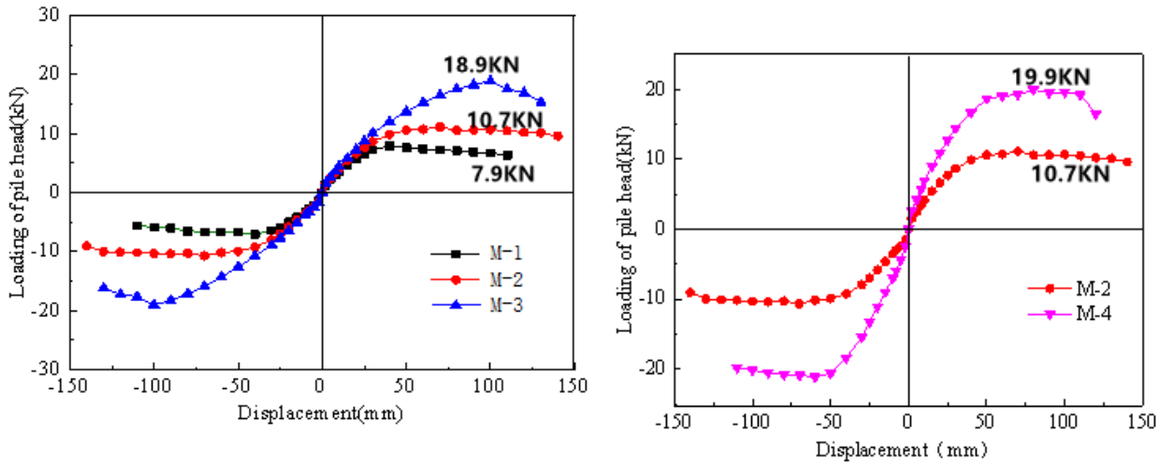

(a) M-1, M-2, M-3 (b) M-2, M-4

Fig – 8: Backbone curves of model piles

Table – 2: Ductility coefficient of the model pile [31]

Number	Y_y (mm)	Y_u (mm)	μ
M-1	22.8	95.2	4.18
M-2	25.3	138.9	5.49
M-3	47.3	129.9	2.75
M-4	27.3	117.9	4.32

As noted in Fig. 8(b), as the displacement increases, the bearing capacity of the rectangular pile (M-4) decreases before the circular pile (M-2), indicating that the circular RC pile has better ductility and energy dissipation performance. Under the condition that the bearing capacity is satisfied, the circular pile has better ductility and is more suitable for IABs with higher seismic requirements and the reinforcement ratio should not exceed 3.2%. Note that, based on the current data, a specific accurate value could not be determined. However, the optimum reinforcement ratio should be between 1.6% and 3.2%.

3.2 Energy Dissipation Performance

The energy dissipation performance is one of the essential indicators of the seismic response of the structure. If the pile is simplified into an elastic beam model, the concrete piles always have the following relationship at different depths in the lateral direction [36-37]:

$$\mu\frac{\partial^2\omega(x,t)}{\partial t^2}+c\frac{\partial\omega(x,t)}{\partial t}+K\omega(x,t)+E_PI\frac{\partial^4\omega(x,t)}{\partial z^4}=0 \quad (1)$$

where μ is the mass density of the pile, c is the damping coefficient of the model pile, K is the soil pressure coefficient of pile-soil interaction, and E_P is the elastic modulus of the pile.

The formula for calculating the energy dissipation of a single pile in this model is as follows [36]:

$$E_{\text{Energy dissipation}}=\int_z^0\int_0^t c\omega(z,t)d\left[\omega(z,t)\right]+\int_z^0\int_0^t K\omega(z,t)d\left[\omega(z,t)\right] \quad (2)$$

Many parameters in the equation cannot be obtained accurately, especially the soil pressure coefficient K in the pile-soil interaction, which changes with the soil type and depth. Furthermore, $\omega(z, t)$ it is not a simple function, and the solution of pile-soil energy dissipation performance is highly complex theoretically. This paper calculates the area of the hysteresis curve under each displacement load and obtains its single-cycle energy dissipation by experiment, then accumulates the energy dissipation of each stage to obtain the cumulative energy dissipation of the RC pile. Fig. 9(a) shows the cumulative energy dissipation of M-1, M-

2, M-3, and M-4 under different displacement loads. The energy dissipation is low when the displacement load is low level. The energy dissipation of the four model piles increased rapidly when the displacement load increased.

Comparing M-1, M-2, M-3, as the reinforcement ratio increases, the energy dissipation of the model pile under the same displacement load increases. When the reinforcement ratio exceeds a critical value (Between 1.6% and 3.2%), the energy dissipation of the model pile decreases as the reinforcement ratio increases. Compared with M-1, the cumulative energy dissipation of M-2 increases significantly, and the capability of energy dissipation increases. However, compared with M-3, for M-2, the energy dissipation of the pile and the reinforcement ratio are negatively correlated. The capability of energy dissipation of M-3 is lower than M-2. It can be seen clearly from comparing M-2 and M-4 that the energy dissipation capacity of the circular piles is superior to rectangle piles, which indicated that the seismic resistance performance of the circular pile is superior to the rectangle pile when the pile be used to the bridge foundation.

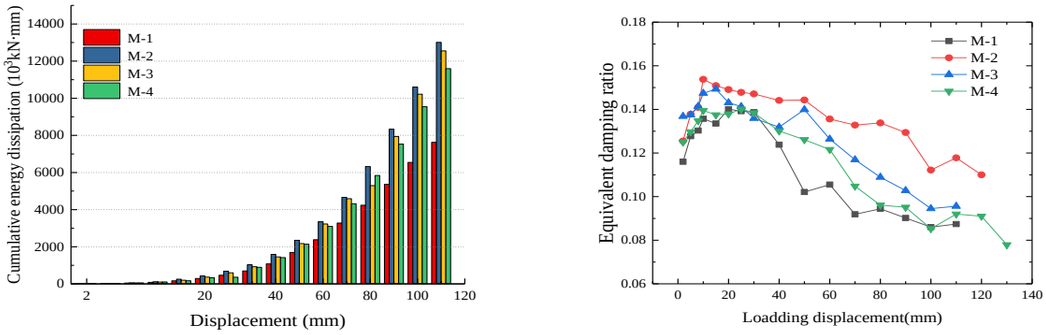

(a) Cumulative energy dissipation (b) Comparison of equivalent damping ratio

Fig – 9: Cumulative energy dissipation and comparison of equivalent damping ratio of the models

The equivalent viscous damping ratio is used to evaluate the energy dissipation capacity of the system [38]. For a typical hysteretic loop, the equivalent viscous damping ratio ξ can be calculated by

$$\xi = \frac{1}{2\pi}\frac{S_{ABCD}}{S_{OFD} + S_{OBE}} \tag{3}$$

where S_{ABCD} is the area of the hysteretic loop and (S_{OFD} + S_{OBE}) is the elastic strain energy stored in the system.

In this experiment, each load grade was repeated three times, and the average of those three cycles was used to calculate the damping ratio. According to Eq. (3), the equivalent viscous damping ratio of the model at each loading grade was calculated. A comparison of the equivalent damping ratios of 4 model piles is shown in Fig. 9(b). Several observations could be made from the diagram: (1) the equivalent damping ratio of RC piles increases as the displacement load increases until reaching maximum value and then decreased, (2) the equivalent damping ratio is between 10% and 20%, which indicates high energy dissipation capacity (pile-soil interaction), and (3) in the range of low reinforcement ratio, the equivalent damping ratio increases as the reinforcement ratio increases (when the reinforcement ratio is outside the range 1.6% to 3.2%, the equivalent viscosity ratio is negatively correlated with the reinforcement ratio), and (4) comparing M-2 and M-4, it is concluded that the seismic resistance performance of the circular pile is superior to the rectangle pile with the same reinforcement ratio.

3.3 Pile Strain

The distributions of compression and tensile strain, tensile strain history, and compressive strain history for the four model piles along the pile depth are shown in Fig. 10. As noted in Fig. 10(a), the distribution of compression and tension strain on both sides of the pile is symmetric and smooth from top to bottom when the top displacement is 2-5 mm for M-1. The tensile strain of the pile is unchanged, and the compressive strain increases until the displacement of pile head to 8 mm, indicating that the pile is within the elastic

strain range. This phenomenon shows that the 5 mm is cracking critical displacement of pile. Other model piles show a similar phenomenon. The critical cracking displacements corresponding to M-2, M-3, and M-4 are 8 mm,10 mm, and 8 mm, respectively, indicating that the reinforcement ratio greatly influences the critical cracking displacement of piles. As the reinforcement ratio increases, the critical cracking displacement increases accordingly. However, the shape of the pile has little influence on the critical cracking displacement.

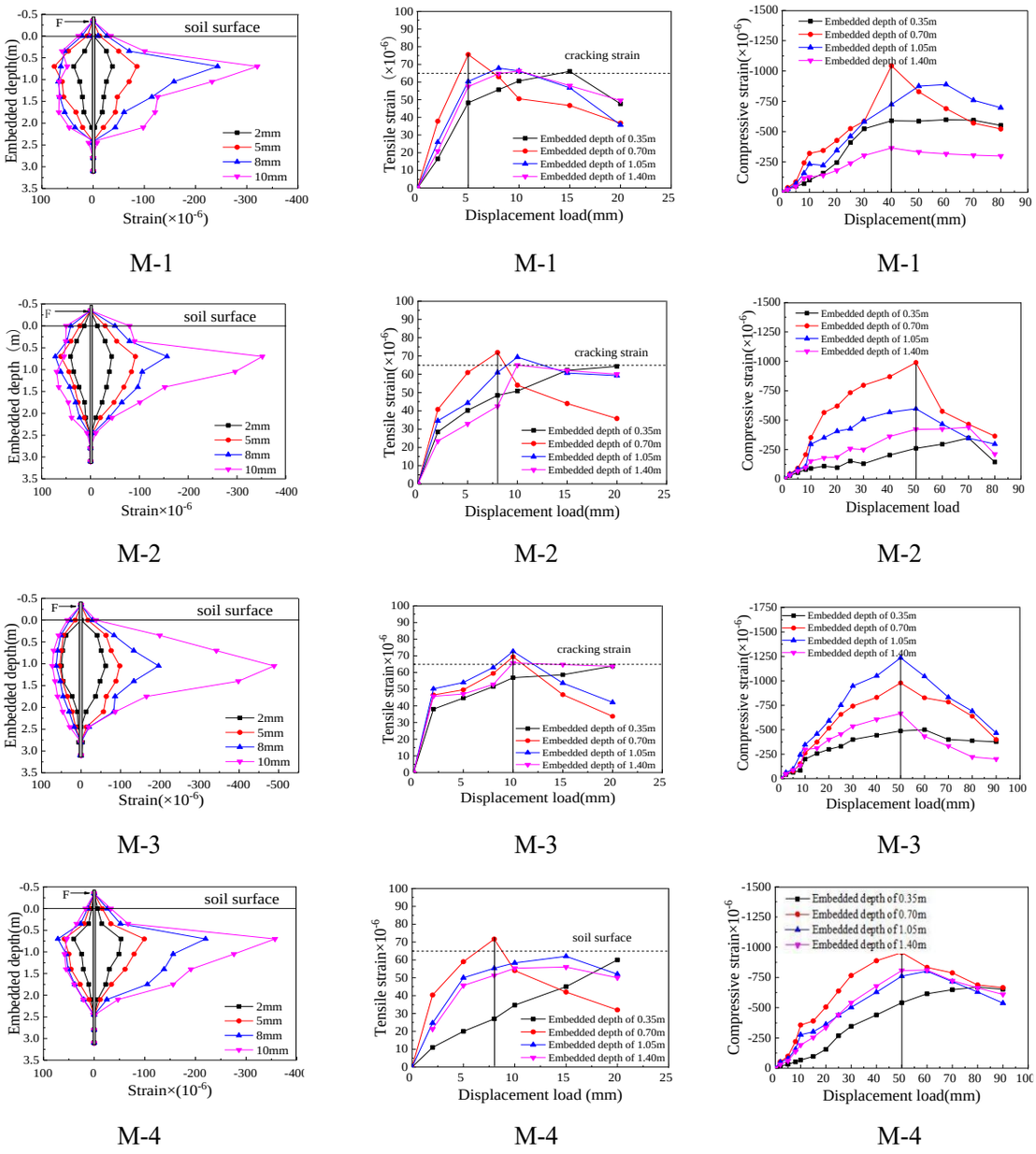

（a）Compressive/tensile strain (b) Tensile strain history (c) Compressive strain history

Fig –10: Strain distribution of the four piles

According to Fig. 10(b), when the displacement load is less than the critical cracking load, the strain increases as the displacement load increases, and the model pile mainly bears the external load. When the applied displacement exceeds the critical cracking displacement, the tensile strains of M-1, M-2, and M-4 drop rapidly at a depth of 0.7 m (4.5 *D*), indicating that this location is the first to crack. The tensile strain of M-3 decreases rapidly at a depth of 1.05 m (6.8 *D*) and 0.7 m (4.5 *D*), indicating that these two positions are the first to crack (Due to the buried position of the strain gauge, the first crack may be between these two points).

Fig. 10(c) shows that when the displacement load is low and the compressive strain of concrete in the

model pile compression area increases significantly. For M-1 and M-2, when the displacement load is over 40 mm (50 mm), the compressive strain of concrete at the buried depth of 0.7 m (4.5 *D*) decreases rapidly, indicating that the concrete was crushed near this area. For M-3 and M-4, when the displacement load is over 50 mm, the compressive strain of concrete at the positions of 0.7 m (4.5 *D*), 1.05 m (6.8 *D*), and 1.4 m (9.0 *D*) decreases rapidly, indicating that concrete was crushed near this area. Compared with M-1 and M-2, the compression damage areas of M-3 and M-4 move down, and the compression damage of M-3 is worse than that of other piles. Because the ratio of reinforcement of M-3 is higher than others, and the bearing capacity of the components is larger. The bearing capacity of the pile also reaches the maximum when the model pile is damaged in the compression area. The increase in the bearing capacity of the model pile is mainly caused by the increase in the lateral resistance of soil around the pile [23, 39]. The bearing capacity of the reinforcement concrete pile also reaches the maximum when the model pile is damaged in the compressed area. Then, the increase in the bearing capacity of the model pile is mainly caused by the increase in the lateral resistance of the soil around the pile.

3.4 Estimation of Bending Moment

The bending moment M of the model piles during the elastic range could be back-calculated from the measured strain under the assumption that the plane section remains plane [25]. The following formula calculates it:

$$M(z) = \frac{EI(\varepsilon_t - \varepsilon_c)}{D} \tag{4}$$

where E is the elastic modulus of concrete, I is the moment of inertia for the section, ε_t is the measured tensile strains at the outmost edge of the section, ε_c is the measured compressive strains at the outmost edge of the section, D is the diameter of the model pile.

Fig.11 shows that the bending moment distributions of the four model piles are similar: the bending moment increases first and decreases after the maximum value. The maximum bending moment of M-3 appeared at a depth of 1.05 m (6.7 *D*), and the other three piles reached the maximum bending moment at a depth of 0.7 m (4.5 *D*). The maximum bending moment of the four model piles also increases continuously to form a plastic hinge point when the displacement load increases.

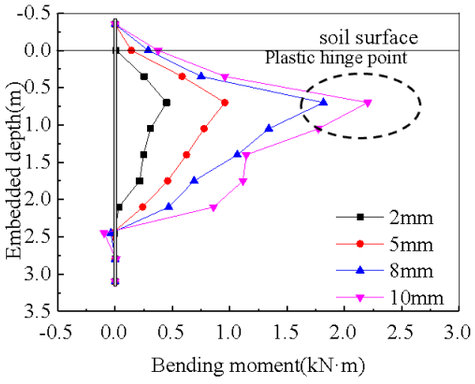

(a) M-1

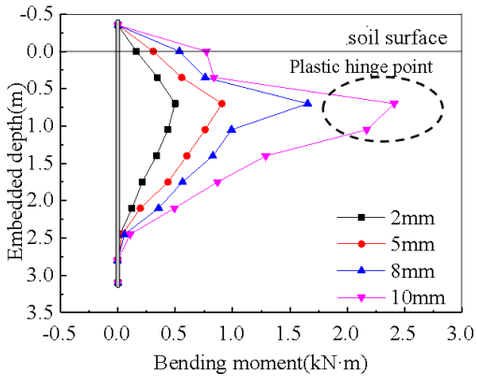

(b) M-2

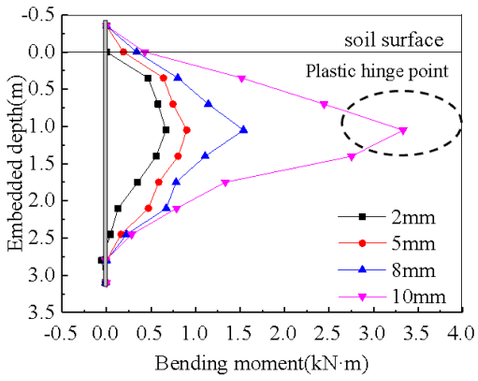

(c) M-3

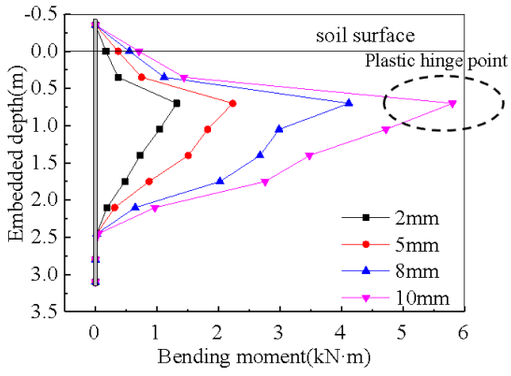

(d) M-4

Fig –11: Bending moment of the pile

To visually reflect the contribution of each model pile to resist the lateral load, the concept of pile bearing ratio is introduced, which is the measured bending moment divided by the pile head lateral-force bending moment. The history of the four piles bearing ratios with a displacement load of 2 mm -10 mm shows that the bearing ratios of the four groups of model piles in the elastic range are more than 50%, indicating that the lateral resistance is mainly borne by the RC pile in the pile-soil system. When the displacement load of the pile exceeds the critical values of 5 mm, 8 mm, 10 mm, and 8 mm, the soil around the pile plays an important role in resisting the external load in the pile-soil system, and the pile-soil interaction is remarkable at this stage. Comparing M-2 and M-4, the pile bearing ratio of the circular pile is less than the rectangular pile. The rectangular pile relies on the pile to bear the external load compared to the circular pile. The results show that the circular pile could increase the area with the pile-soil interaction, which is beneficial to the system energy dissipation.

3.5 Displacement of Model Pile

The displacement of pile is obtained by strain in conventional soil-pile interaction test, the theoretical formula as follows [40, 41]:

$$y'' = -\frac{M(z)}{EI} \tag{5}$$

$$EIy(z_k) = -\int_0^k [\int_0^k M(z)dz]dz + A_1 z + A_2 \tag{6}$$

Substituting Eq. (4) into Eq. (6), the relationship between the displacement y(zk) and the strain ε is derived as:

$$y(z_k) = \int_0^k [\int_0^k \frac{\varepsilon_t - \varepsilon_c}{D} dz]dz + A_1 z + A_2 \tag{7}$$

where $y(z_k)$ is the displacement of the model pile, and A_1, A_2 are constants.

This paper obtained precise displacement dates of the pile by using the method mentioned above. Fig. 12 shows the displacement of points along the pile for displacement load values of 2 mm, 5 mm, 8 mm, 10 mm, 15 mm, and 20 mm, which. As noted, the model piles M-1, M-2, M-3, and M-4 have a sizeable positive displacement near the soil surface to a depth of 1.2 m (7.9 *D*).

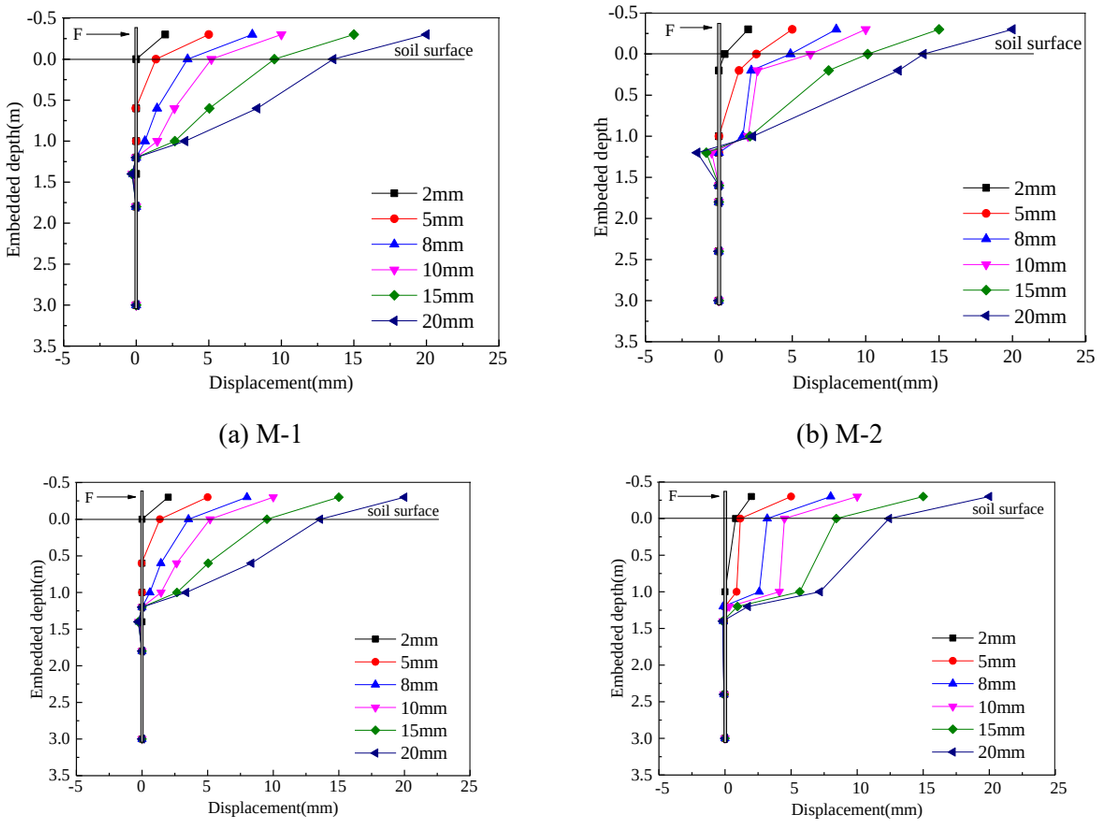

(a) M-1 (b) M-2

(c) M-3 (d) M-4

Fig – 12: Deformed shape of the model pile

Among the 1.2 m (7.9 *D*) to 1.6 m (10.7 *D*), there are reverse displacements of four model piles, and the M-1 and M-2 model piles have larger reverse displacements at this interval, while M-3 and M-4 have smaller displacements within the interval. The reason for this phenomenon is that the reinforcement ratio of M-1, M-2 is lower than M-4, which stiffness is lower than M-4. Comparing M-1, M-2, and M-4, the stiffness of M-4 is larger than M-1, M-2 due to the section of that rectangular pile is larger than the circular pile. The displacement of the model pile under 1.6 m (10.7 *D*) is ignored because pile-soil interaction constraints are strengthened with the depth increases.

According to Figure 13, the failure types of circular piles with different reinforcement ratios show that there are three stages of M-1 in the loading to damage: (1) The elastic stage. In which the pile deformation is elastic, (2) Elastoplastic stage. In this stage, the pile achieves yield deformation, and the deformation is irreversible, and (3) Failure stage. The pile was destroyed in this stage. Compared with M-1, there are four stages in M-2 deformation. Unlike M-1, M-2 has a plastic strengthening stage after the elastoplastic stage. The plastic strengthening stage maintains high resistance when the displacement load is between 50 mm and 110 mm. Like M-1, the M-3 deformation is divided into three stages. Compared with the three deformation curves above, it could be concluded that M-1 and M-3 belong to brittle failure and M-2 belongs to ductile failure. The pile mainly provides the lateral resistance of the pile in the elastic stage. During the elastoplastic and plastic strengthening stage, the lateral resistance of the pile is borne by the pile and pile-soil interaction. In contrast, the pile-soil interaction's lateral resistance is completely provided in the failure stage, and the lateral resistance drops rapidly. The plastic strengthening stage of M-1 is not apparent due to the low reinforcement ratio. M-3 also is not conspicuous with the plastic strengthening stage because of the high reinforcement ratio.

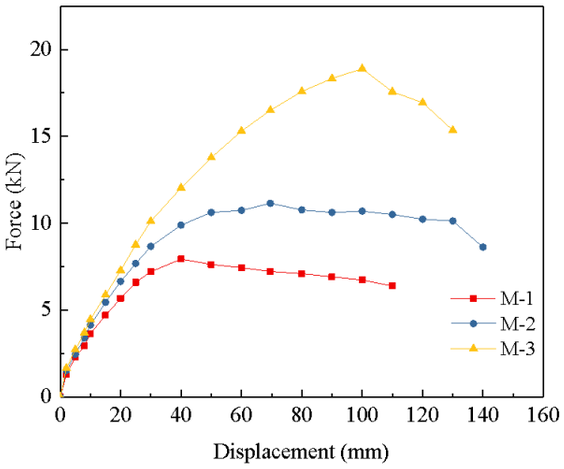

Fig –13: Force-displacement curve of circular pile

3.6 Analysis of Pile Damage

After the test completion, the model pile was removed from the container to observe the pile damage, as shown in Fig. 14. As noted in Fig. 14(a), that there are three cracks in M-1. The first crack appeared under the soil surface at 2.8 *D*, and the second crack appeared at 3.5 *D* under the soil surface. The concrete was severely crushed and destroyed, the reinforcement was exposed, and some of the bars broke. The third crack appeared in 4.5 *D* under the soil surface. It can be seen three cracks in M-2, as shown in Fig 14(b), the first crack appears at a depth of 2.9*D* and the second crack appears at a depth of 3.6 *D*, which area damage is severe, the reinforcement is exposed, and the concrete is crushed. The third crack appears at a depth of 4.6 *D*, where most of the concrete is crushed. M-3 appeared obvious cracks around, as shown in Fig. 14 (c).

The first cracks appeared in the embedded depth of 4.8 *D*, where the cracks appear on the surface of the pile. The second cracks appear in the depth of 5.4 *D*, where the concrete is crushed, and the reinforcement is exposed. The third crack appears at a depth of 6.1 *D*, where the cracks only appear on the surface of the pile. At the same time, there were many vertical cracks between the second and third cracks. The concrete was severely crushed and fell off. The fourth crack appeared at a depth of 6.8 *D*, where the crack only appeared on the pile surface, and no crack through the pile was formed. M-4 appeared three cracks, as shown in Fig 14(d). The first crack appeared in the depth of 3.7 *D*, which appears only on the surface of the pile. The second crack appeared in the depth of 3.7 *D*, where the concrete was severely crushed, and the reinforcement is exposed. Table 2 shows the specific information.

(a) The circular pile (0.8%)

(b) The circular pile (1.6%)

(c) The circular pile (3.2%)

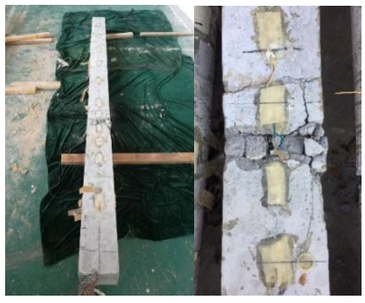

(d) The rectangular pile (1.6%)

Fig – 14: Diagram of the pile failure

Table 3 shows the characteristics of the the model pile damage. As noted, M-3 is the most severely damaged pile. Consistently, the compressive strain of the pile concrete decreases rapidly when the displacement load is over 50mm, indicating that the concrete of the area is crushed. Comparing M-1 and M-2, the compression failure area of M-3 and M-4 moves downward. The damage of M-3 is heavier than other model piles. Meanwhile, the 0.7 m (6.8 *D*) to 1.4 m (4.5 *D*) strain has dropped rapidly by analyzed above in Pile stain, indicating that the area compression damage most seriously. The phenomenon is consistent with the field observation that the pile suffered the most severe damage in the depth of 5.4 *D*, 6.1 *D*, and 6.8 *D*. The pile damage of M-1, M-2, M-4 is also consistent with the theoretical analysis above. Due to space limitations, this paper will not compare and describe the theoretical analysis above and the actual failure situation of each model pile.

Table - 3: Summary of the model pile damage

Number	**Displacement Load Crack**	**Number of Cracks**	**Crack Depth**	**Characteristics of Pile Failure**
M-1	5 mm	3	2.8 *D*	Slight crack of the pile
			3.5 *D*	Concrete was severely crushed
			4.5 *D*	Concrete was crushed
M-2	8 mm	3	2.9 *D*	Slight crack of the pile
			3.6 *D*	Concrete was severely crushed
			4.6 *D*	Concrete was crushed
M-3	10 mm	4	4.8 *D*	Slight crack of the pile
			5.4 *D*	Concrete was severely crushed
			6.1 *D*	Concrete was crushed
			6.8 *D*	Concrete was crushed
M-4	8 mm	3	3.7 *D*	Slight crack of the pile
			4.8 *D*	Concrete was severely crushed
			6.2 *D*	Concrete was crushed

4. CONCLUSIONS

This paper has experimentally investigated the mechanism and deformation of circular and rectangular reinforced concrete piles of integral abutment bridges. Pseudo-static tests of the RC piles under low-cyclic loading were conducted to simulate the periodic displacement of the IAB due to temperature changes. A lateral displacement load was applied on the pile head and the characteristics of energy dissipation, strain, bending moment, lateral displacement, and pile damage were analyzed. Based on this study, the following comments are offered:

1. The results show that the shape of the RC piles hysteresis curve is the spindle, which has a high energy dissipation capacity and lateral displacement resistance capacity. Therefore, RC piles could be used for integral abutment bridges in seismic areas.

2. The energy dissipation performance of the RC piles can be improved by increasing the reinforcement ratio. The energy dissipation and ductility of the circular RC pile are better than those of the rectangle RC pile when other conditions are equal. The ratio of reinforcement of 1.6% to 3.2% is suitable for the RC pile since it provides excellent energy dissipation and ductility.
3. As the reinforcement ratio increases, the yield displacement of the pile can be improved to some extent. Meanwhile, the deformation performance can be improved. However, the pile is restrained by the surroundings due to the deep burial of the pile in the soil, which improves the pile's deformation performance (pile-soil system). The lateral resistance of the RC pile accounts for over 50% of the entire soil-pile system in the elastic stage. However, the resistance distribution of the surrounding soil of the pile is more than 50% in the latter stages.
4. The failure of the RC model pile has regularity with a low cyclic lateral load. The model pile damage is mainly concentrated between 3 *D* and 7 *D,* like the findings for SJABs by Chen et al. [29]. Moreover, a similar buried depth has the same damage features in the coarse sand.
5. Circular piles are recommended for the design of bridges when the RC piles are used as the foundation of integral abutment bridges, especially in areas with high seismic fortification levels. Future research may be conducted to simulate real earthquake using shaking table test. In addition, the pile-soil interaction for multiple-layer soils can be explored along with different conditions of the pile head (free, semi rigid, and fix).

ACKNOWLEDGMENTS

The authors are grateful to anonymous reviewers for their thorough and most helpful comments. This project is financially supported by the Natural Science Foundation of China (Grant Number 51778147).

NOTATION

The following symbols are used in this paper:

S = similar ratio of model test
L_m = model pile diameter
L_p = diameter of the Prototype pile
S_E = similarity ratio *of* the elastic modulus
S_{P0} = similarity ratio of the initial mass density
ω = natural moisture content
e = void ratio of the sand
φ = internal friction angle of the soil
M= mass density of the pile
C= damping coefficient of the model pile
K = soil pressure coefficient of pile-soil interaction
EP = elastic modulus of the pile
ξ = equivalent viscous damping ratio
E = elastic modulus of concrete
I = moment of inertia for the section
ε_t = measured tensile strains at the outmost edge of the section
ε_c =measured compressive strains at the outmost edge of the section
D =diameter of the model pile
$y(z_k)$ = displacement of the model pile
$A1$, $A2$ = constants.

REFERENCES

[1] Ministry of Housing and Urban-Rural Development of the People's Republic of China. Seismic code for building tests (2015). China Building Industry Press.

[2] Girion, D.D., Hawkinson, T. R., Greimann, L. F. (1991). Validation of Design Recommendation for Integral-abutment Piles. *Journal of Structural Engineering* 117(7), 2117-2134, DOI: 10.1061/(ASCE)0733-9445(1991)117:7(2117).

[3] Far, N. E., Maleki, S., Barghian, M. (2015). Design of integral abutment bridges for combined thermal and seismic loads. Earthquakes and Structures, 9(2), 415-430, DOI:10.12989/eas.2015.9.2.415

[4] Salman, N. N., & Issa, M. A. (2019). Displacement Capacities of H-Piles in Integral Abutment Bridges. Journal of Bridge Engineering, 24(12), 04019122. DOI:10.1061/(ASCE)0733-9445(1989)115:11(2914)

[5] Gama, D.A., Almeida, J.F. (2014). Concrete Integral Abutment Bridge with Reinforced Concrete Pile. *Structural Concrete* 15(3), 293-304, DOI: 10.1002/suco.201300081

[6] Abendroth, R.E., Greimann, L.F., LaViolette, M.D. (2007). An integral abutment bridge with precast concrete piles (No. IHRB Project TR-438).

[7] Magbool, H. M. (2019). Analysis of FRP-Wrapped Concrete Piles in Integral Abutment Bridges Subjected to Axial and Cyclic Lateral Loads.

[8] Hong, J.X., Peng, D. W. (2002). Research on the loaded property of integral abutment bridges with flexible piles. *China Journal of Highway and Transport* 15(4), 43-48,

[9] Zhuang, Y.Z., Huang, F.Y., Qian, H.M., Xiong, Z.H. (2017). Pseudo-static Test Research on Mechanic Behavior of PHC Piles with Soil-pile Interaction. *China Journal of Highway and Transport* 30(4), 42-51, DOI: 10.3969/j.issn.1006-3897.2017.04.006

[10] Ministry of Transport of the People's Republic of China (2015). General Specifications for Design of Highway Bridge and Culverts. China Communications Press, Beijing, P.R. of China.

[11] Ministry of Construction of the People's Republic of China (2008). Technical Code for Building Pile Foundation. China Architecture & Building Press.

[12] Huang, F.Y., Zhuang, Y.Z., Fu, C, Qian, H.M., Chen, B.C. (2015). Review on the seismic performance and simplified design method of jointless bridge. *Earthquake Engineering and Engineering Vibration* 1(5), 15-22, DOI: CNKI: SUN:DGGC.0.2015-05-003

[13] Makris, N., Gazetas, G. (1992). Dynamic pile-soil-pile interaction. Part II: Lateral and seismic response. *Earthquake Engineering & Structural Dynamics* 21(2), 145-162, DOI: 10.1002/eqe.4290210204

[14] Mylonakis, G., Nikolaou, A., Gazetas, G. (2015). Soil-Pile-Bridge Seismic Interaction: Kinematic and Inertial Effects. Part I: Soft Soil. *Earthquake Engineering & Structural Dynamics* 26(3), 337-359, DOI: 10.1002/(SICI)1096-9845(199703)26:3<337::AID-EQE646>3.0.CO;2-D

[15] Anoyatis, G., Laora, R.D., Mandolini, A. (2013). Kinematic response of single piles for different boundary conditions: Analytical solutions and normalization schemes. *Soil Dynamics & Earthquake Engineering* 44(1), 183-195, DOI: 10.1016/j.soildyn.2012.09.011

[16] Chidichimo, A., Cairo, R., Dente, G. (2014). 1-g Experimental investigation of bi-layer soil response and kinematic pile bending. Soil Dynamics & Earthquake Engineering 67, 219-232, DOI: 10.1016/j.soildyn.2014.07.008

[17] Shamsabadi, A., Rollins, K. M., Kapuskar, M. (2007). Nonlinear Soil–Abutment–Bridge Structure Interaction for Seismic Performance-Based Design. Journal of Geotechnical & Geoenvironmental Engineering 133(6), 707-720, DOI:10.1061/(ASCE)1090-0241(2007)133:6(707)

[18] Govindaraju, L., Babu, R. R., Taylor, G. (2020). Shake table studies on the dynamic response of pile supported framed structure in soft soil. Civil Engineering and Architecture, 8(6), 1313-1324.DOI：10.13189/cea.2020.080615

[19] Chung, S.G., Kim, S.R., Dung, N.T. (2009). Appraisal of true resistance of PHC piles driven in thick,

soft deposit. International Forum on Strategic Technology. IEEE 109-112, DOI: 10.1109/IFOST.2007.4798533

[20] Park, H., Lee, S. R., Yoon, S. (2013). Evaluation of thermal response and performance of PHC energy pile: Field experiments and numerical simulation. Applied Energy 103(1), 12-24, DOI: 10.1016/j.apenergy.2012.10.012

[21] Park, R. (1989). Evaluation of ductility of structures and structural assemblages from laboratory testing = evaluation de la ductilité de structures et de liaisons à partir d'essais en laboratoire. Bulletin of the New Zealand National Society for Earthquake Engineering. DOI：10.5459/bnzsee.22.3.155-166

[22] Huang, F.Y., Qian, H.M., Fu, C, Zhuang, Y.Z. (2018). Displacement-based Simplified Calculation on Soil-pile Interaction of PHC Pipe-piles. China Journal of Highway and Transport 31(3), DOI: 10.3969/j.issn.1001-7372.2018.03.008

[23] Qian, H. (2017). *Experimental study on seismic performance of integral abutment PHC pipe pile foundation*. Doctoral dissertation, Fuzhou University, Fuzhou, Fujian, China.

[24] Zhuang, Y., Huang, F., Qian, H. Xiong，Z. (2017). Quasi-static test of PHC pipe pile-soil interaction [J]. china journal of highway and transport. 2017,30 (4): 42-51,71. DOI: 10.3969/J. ISSN.1006-3897.2017，DOI：10.3969/j.issn.1006-3897.2017.04.006

[25] Wang, S. (2015*). Study on dynamic performance and energy dissipation capacity of reamed micro-piles in earthquake-resistant semi-integral bridges*. Fuzhou University, Fuzhou, Fujian, China.

[26] Murugan, M, Muthukkumaran, K, Natarajan, C. (2017). FRP-strengthened RC piles. II: Piles under cyclic lateral loads. *Journal of Performance of Constructed Facilities*, (3), Doi:10.1061/(ASCE)CF.1943-5509.0000964.

[27] Zhao, R. Leung, A, Knappett, J, Robinson, S., Brennan, A. (2021). Nonlinear lateral response of RC pile in sand: Centrifuge and numerical modeling. *Journal of Geotechnical and Geoenvironmental Engineering*, (6), Doi:10.1061/(ASCE)GT.1943-5606.0002514.

[28] Cheng, J., Luo, X., Zhuang, Y., Xu, L., Luo, X. (2019). Experimental study on dynamic response characteristics of RPC and RC micro piles in SAJBs. Applied Sciences, 9(13), 2644.DOI：10.3390/app9132644

[29] Xu, L. (2017). Study on dynamic response characteristics of micro pile foundation based on shaking table test. (Medical dispersion, Fuzhou University).

[30] Ministry of Transport. (2018). Specifications for design of highway reinforced concrete and prestressed concrete bridges and culverts. Beijing, P.R. of China.

[31] Ding, W., Leng, G., Wei, Q., Zhang, X., Zhou, Y., Tian, G. (2011). Introduction of "Rules for Design of Ordinary Concrete Proportion." JGJ55-2011, *Concrete World*, 000(012), 76-79.

[32] Chinese Standard (2012). Technical specification for application of self-compacting concrete. China Architecture & Building Press, JGJ-T 283-2012, Beijing, China, 2012.

[33] Lou, M., Wang, W., Jeikiy, Ma, H. (2000). Influence of soil layer boundary in shaking table model test of soil-structure system. Earthquake Engineering and Engineering Vibration, 20(4),7. DOI：CNKI:SUN:DGGC.0.2000-04-004

[34] China Construction Industry Press (2008). Technical Code for Building Pile Foundation. JGJ94 - 2008). Construction Science and Technology, 38-39. Doi:CNKI:SUN: KJjs.0.2012-Z1-013.

[35] Zhou, Y, Deng, X.S., Qian, H.T., Chun, H.M. (2010). An experimental study of the perforation type triple steel tube Buckling Restrained Brace. China Civil Engineering Journal (9), 77-87.

[36] Chen,Y. (2014).Shaking table test study on micro-scale soil-rock dynamic interaction. Fuzhou: Fuzhou University.

[37] Zhuang, Y., Wang, S., Fan, Z., Chen, B. Han, Y. (2016). Experimental study on seismic performance of reamed micro piles. Journal of Fuzhou University (Natural Science Edition) (04),510-515+523.DOI：10.7631/issn.1000-2243.2016.04.0510

[38] Zhuang, Y.Z., Chen, B.C., Briseghella, X.J. (2016). Design and practice of jointless bridges in China. The 1st International Symposium on Jointless Bridge Fuzhou University, Fuzhou, China, 34-57.

[39] Huang, J. (2014). Experimental study on deformation instability mechanism and grouting reinforcement of plain concrete pile composite foundation under embankment. Doctoral dissertation, Southwest Jiaotong University, China.

[40] Li, Z. (2018). Quasi-static experimental study on displacement-based concrete pile-soil interaction. (Medical dispersion).

[41] Tang, L. (2010). Study on p-y curve model of pile-soil dynamic interaction in liquefaction site. Medical dispersion, Harbin Institute of Technology. DOI：10.7666/d.D268912